

## **Morphotectonics of the Carlsberg Ridge between 62°20' and 66°20'E, northwest Indian Ocean**

K.A. Kamesh Raju<sup>1</sup>, A.K. Chaubey, Dileep Amarnath, and Abhay Mudholkar  
National Institute of Oceanography, Dona Paula, Goa – 403 004, India.

<sup>1</sup> Corresponding author. Tel.: +91-832-2450332; Fax: +91-832-2450609

### **Abstract**

The segmentation pattern of 440 km long section of the Carlsberg Ridge between 62°20'E and 66°20'E, in the northwest Indian Ocean, has been studied using multibeam bathymetry and magnetic data. A well defined transform fault is the only first order discontinuity documented in this section of the ridge. Four segments have been identified based on the topographic fabric, along-axis depth variations and the presence of off-axis traces of transform and non-transform discontinuities. These segments constitute four distinct domains representing magmatic and sparsely magmatic crustal accretion. Magnetic model studies show this section of the ridge is a slow spreading ridge with spreading half rates varying from 11 to 16 mm/yr. Along axis variations in the magnetic anomalies and crustal magnetization, the presence of axial volcanic ridges on the inner valley floor, variations in the depth and geometry of the rift valley, and recovery of mantle derived peridotites from the inner valley floor suggest distinct variations in the accretionary processes along the ridge. It is suggested that the linear section in the east with ridge-parallel topographic fabric, continuous magnetic lineations, and the segment with a shallow valley floor with along-axis ridge propagation fabric, represent a magmatic phase of crustal accretion. The wide rift valley, recovery of mantle rocks, deformed topographic fabric, along-axis depth maxima and discontinuous magnetic lineations documented along the middle part of the ridge and the existence of short ridges east of the transform fault represent sparsely magmatic sections with dominance of tectonic extension.

*Keywords: Carlsberg Ridge, Indian Ocean, swath bathymetry, magnetic anomalies, ridge segmentation, crustal accretion*

## 1.0 Introduction

The Carlsberg Ridge, the northwestern limb of the Indian Ocean Ridge system, defines the plate boundary between the Indian and Somalian plates. The Owen fracture zone in the northwest offsets the ridge axis by about 350 km. Towards the east and south, the trend of the ridge changes from NW-SE to near N-S as it joins the Central Indian Ridge near the equator. Several regional geophysical studies carried out in the Indian Ocean (McKenzie and Sclater, 1971; Schlich, 1982; Royer et al., 1989) provided the general configuration of the ridge. Recent geophysical investigations carried out by Chaubey et al. (1993) and Ramana et al. (1993) have provided updated half spreading rates of 12 to 13 mm/yr from new data.

Studies carried out with multibeam mapping tools over the Mid-Ocean Ridge systems revealed the existence of new families of ridge-axis discontinuities that divide the ridge into smaller segments. The distinct topographic fabric of the ridge and its segmentation largely represent the temporal and spatial interplay of two primary accretionary processes, viz., i) magmatic process that provides the melt to form new oceanic crust, and ii) tectonic process during which deformation, faulting and dismemberment of the crust takes place. It is, therefore, important to identify the contribution of these processes to understand the finer scale evolution of the ridge system. High-resolution geophysical data with off-axis coverage extending to few million years is required to understand the interplay between the magmatic and amagmatic (tectonic) processes that have affected the evolution of the ridge segment. The ridge axis discontinuities primarily divide the ridge axis into smaller segments with varied topographic expressions as a consequence of crustal accretion resulting from discrete spreading cells (Macdonald and Fox, 1990; Shaw, 1992; Sinton and Detrick, 1992). Extensive investigations carried out over East Pacific Rise (EPR) and over the segments of Mid-Atlantic Ridge (MAR) have provided insights into the segmentation pattern and accretionary processes of the fast and slow spreading ridge systems (Macdonald et al., 1991; Scheirer and Macdonald, 1993; Sempere et al., 1990,1993; Smith et al., 1993; Gente et al., 1995; Goslin et al., 1999). Recent investigations over the very-slow South West Indian Ridge (Sauter et al., 2001; Dick et al., 2003) and the ultra-slow Arctic Ridges (Cochran et al., 2002; Michael et al., 2003) have enhanced our understanding of the architecture and accretionary processes of the very-slow and ultra-slow spreading mid-ocean ridges. The ridge systems in the north Indian Ocean are the least explored. The finer scale segmentation pattern of the Carlsberg Ridge remained unknown due to lack of high-resolution investigations using modern geophysical tools.

Studies over a short 100 km long segment by Kamesh Raju et al. (1998) and Mudholkar et al. (2002) have provided the first multibeam swath bathymetry maps of the Carlsberg ridge. This effort has been carried out under the Indian Ridge initiative coordinated by the National Institute of Oceanography, Goa, India. Subsequently swath bathymetry and magnetic data were acquired over 440 km long segment of the Carlsberg ridge under this initiative and provided the first high-resolution images of the ridge. In this paper, we present, the first detailed analysis of the morphotectonic elements of a part of the Carlsberg ridge (Fig. 1a) using the new data from swath bathymetry and magnetics.

## **2.0 Marine Geophysical Data**

Multibeam swath bathymetry and magnetic data acquired during the 114, 154 and 194 cruises of ORV Sagar Kanya (July 1996 to August 2003) are used in the present study. About 440 km long portion of the ridge was surveyed with about 50 km off-axis coverage on either side of the spreading axis. 100% insonification of the seafloor was achieved by spacing the multibeam bathymetry tracks at 3 nautical miles (5.5 km) (Fig. 1b). Total magnetic intensity data was acquired simultaneously with a Geometrics marine magnetometer. A chain-bag dredge was deployed to collect rock samples from the rift valley. Fresh basalts were recovered in majority of the dredge hauls, but at two locations mantle derived rocks were present (Table-1, Fig. 1). An Integrated Navigation System (INS) with GPS MX4400 as the primary control provided the navigation.

MB-System (Caress and Chayes, 1995) was used to process the multibeam bathymetry data. The magnetic data was reduced by subtracting the regional field (IAGA, 2000). GMT software (Wessel and Smith, 1991) was used for plotting and presentation of the data.

## **3.0 Multibeam bathymetry of the spreading centre**

The Carlsberg ridge is characterised by rugged topography, steep valley walls and wide rift valley floor, all characteristics of a slow spreading ridge. There is only one first order segment caused by a well-defined transform fault and fracture zone along the entire length of the surveyed portion of the ridge. The ridge in general is oriented in a NW-SE direction; the gradual bend in the ridge axis is accommodated by non-transform discontinuities and along-axis bathymetric deeps (Fig. 1). Based on characters related to topography, the off-axis trace of the discontinuities, and the presence or absence of ridge-parallel topographic fabric, we have divided the ridge into four segments. We refer these segments as Segment I to IV from west to east (Fig. 1). There are significant variations in the width of the valley floor along the ridge axis. The edge of the inner valley floor is defined as the base of the first major scarp of the bounding wall (Shaw, 1992; Sempere et al., 1993) and the edge cuts across the bathymetric contours, as the scarps are not continuous. The inner valley floor in general is bounded by 3000 m isobath, and is marked by fault scarps. Swath bathymetry maps were used to delineate detailed morphotectonic features.

### **3.1 Along-axis variations**

The along axis bathymetry profile and the identified segments are shown in Figure 2b. It has been well documented that slow-spreading ridges are characterised by shallow segment centres and deeper segment ends (Kuo and Forsyth, 1988; Lin et al., 1990; Shaw, 1992). The ridge segmentation of the surveyed portion of the Carlsberg Ridge differs from that of MAR pattern. The segments over the CR are defined based on pronounced differences in off-axis morphologies and changes in average axial depth. On a wider scale, along-axis bathymetry lows coincide with segment boundaries. The axial depth profile has a peak to trough relief ranging from 500 to 1200 m. Segment I consists of ridge axis with a well defined, near symmetric, axis-parallel topographic fabric limited by a non-transform discontinuity (NTD) at about 3°50'N latitude and 63°10'E longitudes. Segment II represents the ridge section with the deepest valley floor, while the shallowest valley floor is documented in Segment III. A well defined transform fault separates Segment III from Segment IV. The average depth along each segment (Fig. 2) indicates that Segment I and Segment III are shallow (~3500 m)

compared to the average depth (~ 4000 m) observed in Segments II and IV. Segment II is conspicuous with along axis depth maxima ranging from 4500 to 4700 m (Fig. 2 and 3a). The depth maxima observed here represent the deepest parts of the surveyed section of the Carlsberg Ridge. This conspicuous change of about 500 m in the axial valley floor depth is an indicator of magmatic activity. The general morphological configuration of Segment II, with anomalous along-axis valley deeps of 4500 to 4700 m, and of Segment IV with short ridges and average valley floor depth of 4000 m suggest low levels of magmatic supply (Dick et al., 2003; Small, 1998). Segment I with an average valley floor depth of 3800 m and the shallowest valley floor depth of 2900 m observed in Segment III have relatively longer ridge sections without discontinuities. Furthermore, these segments have well-defined ridge-parallel topographic fabric suggesting higher levels of magmatic accretion. Based on these observations we have interpreted Segment I and III as magmatic sections and the Segments II and IV as sparsely magmatic sections.

### **3.2 Magmatic sections**

Segments I and III are considered as magmatic sections of the ridge based on the along axis and off-axis topographic character. The ridge axis in Segment I is predominantly linear with well-defined near symmetrical ridge parallel topographic fabric (Fig. 1). The width of the rift valley varies from 16.8 to 22.8 km with steep valley walls ranging in height from 1837 to 2325 m. The eastern end of the Segment is represented by an NTD that offsets the ridge axis by 6.8 km. Prominent axial volcanic ridges (AVRs) ranging in length of 16 to 23 km are documented in this segment. The 23 km long and 3 km wide AVR is the largest observed along the surveyed part of the ridge. At the eastern end, the AVRs are symmetrically placed on either side of the spreading axis and these are aligned towards south western valley wall near the NTD. The AVRs are the principal sites of lava extrusion (Macdonald and Luyendyk, 1977). Prominent AVRs were identified in wide-ranging morphologies and structures over the northern MAR segments (Sempere et al., 1990; Smith and Cann, 1992; Sempere et al., 1993; Kong et al., 1988). The rift valley floor widens at the NTD and peridotites along with gabbros were recovered from the base of the valley wall in this region (Fig. 1) suggesting a thinner crust exposing the mantle rocks. It is observed that these AVRs become continuous with the valley walls during the course of evolution of the spreading segment. The off-axis fabric is correlatable with the magnetic anomalies. The axis-parallel fabric can be traced until anomaly 2A times, suggesting predominance of uniform crustal accretion.

Segment III is characterized by a linear section of the ridge with a relatively shallow rift valley. Smooth and elevated topography is observed on the flanks of these segments (Fig. 1) suggesting magmatic phase of accretion. Based on morphology, mantle Bouguer anomalies and seismic signatures, the shallower mid sections of the ridge segments are considered as regions of enhanced mantle upwelling (Purdy and Detrick, 1986; Kuo and Forsyth, 1988; Sempere et al., 1990; Lin et al., 1990; Kamesh Raju et al., 1997). The ridge segment is shallowest in the middle at about 3°10'N latitude and 64°48'E longitude (Fig. 1) reaching to 2900 m, whereas at the ends of the segment, depths reach 4000 m. The rift valley is relatively narrow, having a minimum width of 5 km at the shallowest part. A prominent 15 km long, 2.5 km wide, and 700 m high AVR is located in the middle of the inner valley floor (Fig. 6). The off-axis topography in this segment is dominated by oblique trending topographic fabric formed by the termination of abyssal hill topography. These lineations defined by the

termination of abyssal hill topographic highs resemble the bathymetric fabric generated by the propagating ridge (Hey et al., 1980, Cormier and Macdonald, 1994; Carbotte et al., 1991). Bathymetric lows of about 300 m are observed (Fig. 6) on the flanks associated with oblique topographic fabric. These lows resulted from the termination of abyssal hill topography on the ridge flanks and probably represent the outer and inner pseudo faults. Magnetic lineations in this region have also shown offsets corresponding to the oblique trending topographic fabric. Towards its eastern end, the segment is bounded by a first order discontinuity defined by a transform fault at 65°18'E longitude that offsets the ridge axis by 19.2 km. The transform fault joins the deeps of 3900 m and 4200 m at the end of the segment and trends at 40°N. The fracture zone associated with the transform fault is well developed and can be identified both on swath bathymetry and the satellite gravity image. The well-defined off-axis trace of the fracture zone suggests long-lived subsurface partitioning.

### **3.3 Sparsely magmatic sections**

Segments II and IV represent sparsely magmatic sections of the ridge. Segment II constitutes a broad deformed zone defining a bend in the ridge axis (Fig. 1). The chaotic, blocky topographic fabric with less symmetry with respect to the ridge axis characterises this segment. The deformation of the seafloor can be seen off axis. The rift valley is about 25 km wide around 3°45'N latitude and 63 ° 45'E longitudes. Mantle derived serpentinites were recovered near this region (Fig. 1). Axial volcanic ridges are present at the base of the valley walls on the inner valley floor. Recovery of mantle derived serpentinites suggest thin-crust domain resulting from poor magma supply. The anomalous along-axis deeps observed along this segment (Fig. 2b) indicate crustal thinning. The thin-crust domains were found to have rugged topography (Cannat et al., 1995). Recovery of mantle derived ultramafics at 15°N region of MAR was attributed to low magma supply (Cannat et al., 1997). Segment IV consists of an en-echelon pattern of short ridges east of the transform fault at 65°18'E (Fig. 6). Prominent AVR's rise to about 800 m from the inner valley floor on either side of the spreading axis (Fig. 6).

## **4. Magnetic anomalies and magnetization**

Along-track plot of the magnetic anomalies (Fig. 3) depict a well-defined central anomaly that displays variations along the axis and identifiable magnetic lineations on either side of the ridge axis. Seafloor spreading magnetic model studies have been carried out to identify the magnetic anomalies and to assign the spreading rates. Synthetic anomalies are generated with variable spreading rates, using the time scale of Cande and Kent (1995), and assuming 500 m thick blocks with 0.01 A/m magnetization. The model studies indicate variable and asymmetric spreading rates ranging from 11 mm/yr to 16 mm/yr (half rate) (Fig. 4). Magnetic anomalies reduced to the pole are presented along selected profiles together with the bottom topography and crustal magnetization (Fig. 4).

In Segment I, the linear trend of anomalies can be correlated with the ridge-parallel topographic fabric. The width of the central anomaly varies between 20-30 km and the amplitude from 150-330 nT. High amplitude and high wave-length anomalies are observed near NTD. Serpentinites and peridotites were recovered in a dredge sample from the rift valley wall at the NTD. The average half spreading rate in this segment, along profile P1 is 12 mm/yr to the southwest, and 15 mm/yr to the northeast (Fig. 4). The bend in the ridge axis in Segment II is reflected in the magnetic signature. The

central anomaly is generally wide in this segment, ranging from 29 to 36 km (Fig. 3), with amplitudes ranging from 180 to 400 nT. The magnetic lineations of J and 2 are not continuous while anomaly 2A is well documented and can be correlated. The off-axis topographic fabric does not show ridge parallel fabric and appears to be disturbed until anomaly 2A. The ridge-parallel fabric can be seen beyond anomaly 2A. The seafloor spreading magnetic model studies carried out over the profiles suggest asymmetric spreading with higher spreading rates over the NE flank for the segments I, II and III. The spreading rate is higher over the SW flank for the Segment IV east of the transform fault (Fig. 2d).

In Segment III, offsets of the order of 4 km are documented in the magnetic lineations, which correspond to the oblique trending topographic fabric observed here. The topographic fabric and the magnetic signatures suggest ridge propagation. The magnetic lineations show offsets corresponding to the bathymetric lineations; these offsets are better developed on the north-eastern ridge flank among the anomalies 2 and 2A with an offset distance of about 4 km (Fig. 3). On the south western flank, a noticeable offset is observed only across the magnetic lineation 2A, the magnetic lineation representing anomaly 2 terminates corresponding to the flank topographic high. Magnetic lineations show prominent offsets across the transform fault and the fracture zone. High intensity magnetic anomalies are noticed over the AVRs identified from swath bathymetry. Spreading rates determined from seafloor-spreading model studies carried out along the profiles P4 and P5 over Segment III indicate average half spreading rate varying from 11 to 12.8 mm/yr on P4 and 15 to 15.5 mm/yr on P5. The average spreading rate along the segments for the NE and SW flanks is depicted along with the along axis depth profile (Fig. 2d).

Segment IV is characterised by a well-defined central anomaly that has amplitudes ranging from 375 to 520 nT and width ranging from 25 to 40 km. Magnetic lineations of anomalies J, 2 and 2A are identified on the both sides of the ridge axis. Seafloor spreading model studies indicate half spreading rates of 15.5 mm/yr on the south western flank and 13.4 mm/yr on the north eastern flank for profile P6. Asymmetry in spreading indicated by the difference in half spreading rate is high in Segment I and Segment IV. Segment I and III displayed higher spreading rates on north-eastern side while in Segment IV the spreading rate is higher on the south-western side (Fig. 2d).

To obtain source magnetization, we carried out three-dimensional inversion of the magnetic data using the Fourier transform method (Parker and Huestis, 1974; Macdonald et al., 1980). The multibeam bathymetry at a grid spacing of 980 m was used for the inversion assuming a constant 500 m thickness for the source layer. Taylor expansion up to fifth order was carried out, 5 iterations brought sufficient convergence. The resultant magnetization solution (Fig. 5) shows well defined magnetization stripes corresponding to the normal and reversely magnetized crust. Since we assumed constant thickness of magnetized layer in the inversion, regions of higher magnetization in the solution may also represent thickening of the source layer. Variation in magnetization along the profiles is presented along with the bathymetry and seafloor spreading model (Fig. 4). The central anomaly is associated with positive magnetisation. High magnetizations are observed over the AVRs identified based on swath bathymetry. High magnetization characterises the along-axis signature and the segment ends have shown low magnetization (Fig. 2b). The magnetization variations

along the profile coinciding with anomaly 2A period display more uniform variations and correlate well with topography (Fig. 2a and 2c).

## 5. Summary and Discussion

The general morphology of the Carlsberg ridge surveyed in the present study is similar to the MAR between Kane and Atlantis transforms. No transform offset was observed over the 800 km long MAR between Kane and Atlantis transforms. Instead the ridge axis is offset by non-transform discontinuities that are usually located at the local depth maxima (Sempere et al., 1990, 1993). Segments II and III having well defined boundaries are about 130 km long, indicating longer segment lengths probably due to the absence of first order discontinuities. No major discontinuities were documented over the surveyed section of the Carlsberg ridge, except a small offset transform at 65°18'E longitude (Fig. 6). It is noted that even though on a wider scale the along-axis bathymetric lows coincide with the segment ends, not all the along-axis lows correspond to segment ends (fig. 2b). This observation suggests that the segmentation pattern over the Carlsberg Ridge is not precisely the same as defined along the MAR.

The well defined ridge-parallel topographic fabric over Segment I represents a magmatic section. Segment II is conspicuous with anomalous deeps, wide asymmetric rift valley, poorly developed AVRs, and blocky and chaotic topographic fabric, suggesting sparsely magmatic phase. This segment is similar to the ridge segment north of 15°20'N fracture zone over the MAR (Fujiwara et al., 2003). The shallow valley floor with propagating ridge features on the flank topography observed over Segment III indicate a volcanic section of the ridge with dominant magmatic accretion. The section with short segments east of the transform fault suggests less magmatic phase with a predominant tectonic extension. The morphological expressions observed are similar to the slow, very-slow and ultra-slow spreading ridge segments (Sempere et al., 1993; Sauter et al., 2001; Fujiwara et al., 2003; Michael et al., 2003).

Off-axis traces oblique to the ridge-parallel topographic fabric, defined as discordant zones that form V-shaped bathymetric lineaments, were observed over the MAR (Rona et al., 1976; Rona and Gray, 1980; Tucholke and Schouten, 1988). The V-shaped discordant zones between the Kane and Atlantis transforms over the MAR were interpreted as northward migrating non-transform offsets over the last 2 Ma (Sempere et al., 1993). We interpret the oblique bathymetric lineaments defining the termination of the abyssal hill topography as resulting from propagating ridge following the analogy of Kleinrock et al. (1997). In case of migration of non-transform offsets, well-developed bathymetric lows corresponding to the NTDs were observed. Propagation rate is computed by using the acute angle between the propagating ridge and the pseudofaults that are oblique to the ridge axis, and the half spreading rate (Kleinrock et al., 1997). The computed propagation rate of the observed propagator in the present study is 17 mm/yr. Rift propagation was widely observed along the slow spreading Mid-Atlantic Ridge (Brozena and White, 1990; Carbotte et al., 1991; Sempere et al., 1995). The ratio of propagation rate to half spreading rate has been used to classify the propagators into fast and slow propagators (Kleinrock et al., 1997). The reported ratios for slow spreading MAR are less than 0.5, while the ratio of propagation to half spreading rate as high as 10 was observed on the fast spreading East Pacific Rise. Fast rift propagators with ratios in excess of 2

were reported by Kleinrock et al. (1997) for a segment on MAR near 26°N. The computed ratio in the present study is 1.3. By analogy with the MAR, we classify the identified propagator over the Carlsberg ridge segment as an intermediate rate propagator.

Several mechanisms have been suggested to cause the rift propagation including concentration of gravity sliding stresses, greater propagation likelihood for longer cracks, changes in direction of seafloor spreading and motion of the ridge in an absolute reference frame. Residual gravity anomalies observed over MAR are interpreted as representing episodic supply of magma to the ridge (Lin et al., 1993; Tucholke et al., 1997). The plate separation is dominated by magmatic intrusion during higher magma supply reflected by the gravity lows, and is accommodated by faulting during amagmatic phases. It is suggested that rift propagation may develop during the transition from more magmatic periods of spreading to less magmatic periods of spreading. In a slow spreading rift with co-existing sections of magmatic and amagmatic ridge zones, it is possible that the propagation tends to migrate toward the less magmatic zone. The ridge propagation is observed to be towards the less magmatic zone that has relatively thinner crust in the case of NTD observed in Segment I and the propagating fabric observed in Segment III. The NTDs in Segment IV are not sufficiently mapped to define such characterisation. The propagators transect individual rift segments but do not extend to neighbouring segment, as rifting of thicker lithosphere encountered across the segment-end transform is more difficult.

The cause of variations in along-axis bathymetry appears to be controlled by the magmatic activity. The along-axis deeps and chaotic blocky topography observed over Segment II contrast with the symmetrical topographic fabric observed over Segment I and III. The topographic fabric suggest fault controlled structures in Segment II indicating lower supply of magma resulting in thinner crust as opposed to the relatively more organised smoother topographic fabric observed over Segments I and III indicating higher magma supply.

The magnetic signatures closely followed the seafloor morphology, reflecting variations in response to the emplacement of AVRs and the magmatic and amagmatic sections of the ridge. High intensity magnetic anomalies ranging from 300 to 450 nT and high magnetizations represented the AVRs noticed on the swath bathymetry. Well-defined and easily identifiable and correlatable linear magnetic anomalies characterise the magmatic sections. A wider central anomaly and highly discontinuous lineations represent the less magmatic sections that are undergoing dominant tectonic extension. The offsets in the magnetic lineations in Segment III together with topographic fabric support the propagating ridge proposition. Offsets in magnetic lineations are noticed extending up to the lineation defining anomaly 2A, suggest that the along axis propagation has been active since the last 2-3 Ma.

## **6. Conclusions**

The 440 km long section of the Carlsberg ridge is predominantly comprised of non-transform discontinuities with along-axis depth maxima of ~ 4700 m and a single transform discontinuity. The morphotectonic character of the ridge with wide rift valley (13-26 km), and axial volcanic ridges (AVRs) ranging in heights 200-800 m, length 5-23 km, is similar to the segments of the northern MAR, but with distinctly different segmentation pattern controlled by non-transform discontinuities.



It is suggested that the linear ridge section in Segment I with ridge-parallel topographic fabric, continuous magnetic lineations, and Segment III having a shallow valley floor and along-axis ridge propagation fabric represent ridge segments that are undergoing magmatic accretion.

A wide rift valley, recovery of mantle rocks, deformed fabric, along axis depth maxima and discontinuous magnetic lineations along Segment II suggest sparsely magmatic section. Short ridges constituting Segment IV, east of the transform fault with deformed topographic fabric, and the deep valley floor also suggest sparsely magmatic zone with dominance of tectonic extension.

Magnetic lineations are continuous and well defined along the magmatic sections and discontinuous along the amagmatic sections undergoing tectonic extension. Offsets (~4 km) in the magnetic lineations are noticed corresponding to the propagating ridge fabric observed in swath bathymetry, suggesting along axis ridge propagation that has been prevalent since anomaly 2A times.

## **7. Acknowledgements**

We thank Dr. S.R. Shetye, Director, National Institute of Oceanography, Goa, for the encouragement and support given to carry out the study. We are benefitted by the constructive comments of anonymous reviewers. We thank Dr. Piper, Editor-in-chief for the valuable suggestions on refinement of the manuscript. The study was carried out under the CSIR Network program on RIDGEs. Department of Ocean Development, New Delhi is thanked for providing ship time of ORV Sagar Kanya. This is N.I.O. contribution no. 4358

## 8. References

- Brozena, J.M., White, R.S., 1990. Ridge jumps and propagations in the South Atlantic Ocean. *Nature* 348, 149-152.
- Cande S.C., Kent D.V., 1995. Revised calibration of the geomagnetic polarity timescale for the late Cretaceous and Cenozoic. *J. Geophys. Res.* 100, 6093-6095.
- Cannat, M., Mevel, C., Maia, M., Deplus, C., Gente, P., Agrinier, P., Belarouchi, A., Dubuisson, G., Humler, E., Reynolds, J., 1995. Thin crust, ultramafic expousers, and rugged faulting patterns at the Mid-Atlantic Ridge (22°-24°N). *Geology*, 23, 49-52.
- Cannat, M., Lagabrielle, Y., Bougault, H., Casey, J., Nathalie de Coutures, Dmitriev, L., Fouquet, Y., 1997. Ultramafic and gabbroic expousers at the Mid-Atlantic Ridge: geological mapping in the 15°N region. *Tectonophysics*, 279, 193-213.
- Carbotte, S.M., Welch, S.M., Macdonald, K.C., 1991. Spreading rates, rift propagation, and fracture zone offset histories during the past 5 m.y. on the Mid-Atlantic Ridge, 25°-27°30'S and 31°-34°30'S. *Mar. Geophys. Res.* 13, 51-80.
- Caress, D.W., Chayes, D.N., 1995. MB-system, developed at Lamont-Doherty Earth Observatory report.
- Chaubey, A.K., Battacharya, G.C., Murthy, G.P.S., Desa, M., 1993. Spreading history of the Arabian Sea: some new constraints. *Mar. Geol.* 112, 343-352.
- Cochran, J.R., Kurrus, G.J., Edwards, M.H., Coakley, B.J. 2003. The Gakkel Ridge: Bathymetry, gravity anomalies and crustal accretion at extremely slow spreading rates. *J. Geophys. Res.* 108, doi: 10.1029/2002JB001830.
- Cormier, M.H., Macdonald, K.C., 1994. East Pacific Rise 18°S-19°S: Asymmetric spreading and ridge reorientation by ultra-fast migration of axial discontinuities. *J. Geophys. Res.* 99, 543-564.
- Dick, H.J.B, Lin, J., Shouten, H., 2003. An ultraslow- spreading class of Ocean ridge. *Nature* 426, 405-412.
- Fujiwara, T., Lin, J., Matsumoto, T., Kelemen, P.B., Tocholke, B.E., and Casey, J.F., 2003. Crustal evolution of the Mid-Atlantic Ridge near the Fifteen-Twenty Fracture zone in the last 5 Ma. *Geochem. Geophys. Geosyst.* 4, 1024, doi: 10.1029/2002GC000364, 2003.
- Gente, P., Pockalny, R.A., Durand, C., Deplus, C., Maria, M., Ceuleneer, G., Mevel, C., Cannat, M., Laverne, C., 1995. Characteristics and evolution of the segmentation of the Mid-Atlantic Ridge between 20°N and 24°N during the last 10 million years. *Earth Planet. Sci. Lett.* 129, 22-71.
- Goslin, J., Triatnord Scientific party, 1999. Extent of Azores plume influence on the Mid-Atlantic Ridge north of hotspot. *Geology* 27, 991-994.

Hey, R.N., Duenebier, F.K., Morgan, W.J., 1980. Propagating rifts on mid-ocean ridges. *J. Geophys. Res.* 85, 3647-3658.

Hey, R.N., Kleinrock, M.C., Miller, S.P., Atwater, T.M., Searle, R.C., 1986. Seabeam/Deep-Tow investigations of an active oceanic propagating rift system, Galapagos 95.5°W. *J. Geophys. Res.* 91, 3369-3393.

IAGA Division V, working group 8, 2000. International Geomagnetic Reference Field, 2000. *Phys. Earth Planet Inter.* 120, 39-42.

Kamesh Raju, K.A., Ramprasad, T., Subrahmanyam, C., 1997. Geophysical investigations over a segment of the Central Indian Ridge, Indian Ocean. *Geo-Mar. Lett.* 17, 195-201.

Kamesh Raju, K.A., Kodagali, V.N., Fujimoto, H., 1998. Three dimensional gravity and magnetic studies over a segment of the Carlsberg Ridge [abs.], 35th Annual Convention and meeting on Continental Margins of India- Evolution, Processes and Potentials, Indian Geophysical Union, held at NIO, Goa, Nov., 18-20, P29.

Kleinrock, M.C., Tucholke, B.E., Lin, J., Tivey, M.A., 1997. Fast rift propagation at a slow-spreading ridge. *Geology*, 25, 639-642.

Kong, L.S.L., Detrick, R.S., Fox, P.J., Mayer, L.A., Ryan, W.B.F., 1988. The morphology and tectonics of the MARK area from Sea Beam and Sea MARC I observations (Mid-Atlantic Ridge 23° N), *Mar. Geophys. Res.* 10, 59-90.

Kuo, B.Y., Forsyth, D.W., 1988. Gravity anomalies of the ridge-transform system in the South Atlantic between 31 and 34.5° S: Upwelling centers and variations in crustal thickness. *Mar. Geophys. Res.* 10, 205-232.

Lin, J., Purdy, G.M., Schouten, H., Sempere, J.C., Zervas, C., 1990. Evidence from gravity data for focused magmatic accretion along the Mid-Atlantic Ridge. *Nature* 344, 627-632.

Macdonald, K.C., Luyendyk, B.P., 1977. Deep-tow studies of the structure of the Mid-Atlantic Ridge crest near 37° N (FAMOUS). *Geol. Soc. Am. Bull.* 88, 621-636.

Macdonald, K.C., Fox, P.J., 1990. Mid Ocean Ridge. *Sci. Am.* 262 (no.6), 42-49.

Macdonald, K.C., Scheirer, D.S., Carbotte, S.M., 1991. Mid-Ocean Ridge: Discontinuities, Segments and Giant Cracks, *Science* 253, 986-994.

McKenzie, D.P., Sclater, J.G., 1971. The evolution of the Indian Ocean since the Late Cretaceous. *Geophys. J. R. Astron. Soc.* 25, 437-528.

Michael, P.J., Langmuir, C.H., Dick, H.C.B., Snow, J.E., Goldstein, S.L., Grraham, D.W., Lehnert, K., Kurras, G., Jokat, W., Muhe, R., Edmonds, H.N., 2003. Magmatic and amagmatic seafloor generation at the ultraslow-spreading Gakkel ridge, Arctic Ocean. *Nature* 423, 956-961.

Mudholkar A.V., Kodagali V.N., Kamesh Raju K.A., Valsangkar A.B., Ranade, G.H., Ambre N.V. 2002. Geological and geophysical observations along a segment of slow-spreading Carlsberg Ridge. *Curr. Sci.* 82, 2982-989.

Parker, R.L., Huestis, S.P. 1974. The inversion of magnetic anomalies in the presence of topography. *J Geophys. Res.* 79, 1587-1593.

Purdy, G. M., Detrick, R. S., 1986. The crustal structure of the Mid-Atlantic Ridge at 23°N from seismic refraction studies. *J. Geophys. Res.* 91, 3739–3762.

Ramana, M. V., Ramprasad, T., Kamesh Raju, K. A., Desa, M., 1993. Geophysical studies over a segment of the Carlsberg Ridge, Indian Ocean. *Mar. Geol.* 115, 21-28.

Rona, P.A., Gray, D.F., 1980. Structural behaviour of fracture zones symmetric and asymmetric about a spreading axis: Mid-Atlantic Ridge crest (lat 23° N to 27° N). *Geol. Soc. Am. Bull.* 91, 485-496.

Rona, P.A., Harbison, R.N., Bussinger, B.G., Scott, R.B., Natwalk, A.J., 1976. Tectonic fabric and hydrothermal activity of the Mid-Atlantic Ridge crest (lat 26° N). *Geol. Soc. Am. Bull.* 87, 661-674.

Royer, J.Y., Sandwell, D.T., 1989. Evolution of the eastern Indian Ocean since the Late Cretaceous - Constraints from Geosat altimetry. *J. Geophys. Res.* 94, 13755-13782.

Sauter, D., Partriat, P., Jestin, C.R., Cannet, M., Brias, A., Gallieni Shipboard Scientific Party, 2001. The Southwest Indian Ridge between 49°15'E and 57°E: focused accretion and magma redistribution. *Earth Planet. Sci. Lett.* 192, 303-317.

Scheirer, D.S., Macdonald, K.C., 1993. Variation in cross-sectional area of the axial ridge along the East Pacific Rise: Evidence for the magmatic budget of a fast spreading center. *J. Geophys. Res.* 98, 7871-7885.

Schlich, R., 1982. The Indian Ocean: Aseismic ridges, spreading centers, and oceanic basins, in: A. E. M. Nairn and F. G. Stehli (Eds.), *The Ocean Basins and Margins*, vol. 6, The Indian Ocean, Plenum, New York, pp. 51–147.

Sempere, J.C., Nine Others., 1995. The Mid-Atlantic Ridge between 29°N and 31°30'N in the last 10 Ma. *Earth Planet. Sci. Lett.* 130, 45-55.

Sempere, J.C., Lin, J., Brown, H.S., Schouten, H. Purdy, G.M., 1993. Segmentation and Morphotectonic variations along a Slow –Spreading Center: The Mid-Atlantic Ridge (24°00'N- 30°40'N). *Mar. Geophys. Res.* 15, 153-200.

Sempere, J.C., Purdy, G.M., Schouten, H., 1990. The segmentation of the Mid-Atlantic Ridge between 24°N and 30°40'N. *Nature* 344, 427-431.

Shaw, P.R. 1992. Ridge segmentation, faulting and crustal thickness in the Atlantic ocean. *Nature* 358, 490-493.

- Sinton, J. M., Detrick, R. S., 1992. Mid-Ocean Ridge Magma Chambers. *J. Geophys. Res.* 97, 197–216.
- Small, C., 1998. Global systematics of Mid Ocean Ridge morphology, in: Buck, W., Delaney, P.T., Karson, J.A., Lagabriele, Y. (Eds.), *Faulting and Magmatism at Mid-Ocean Ridges.*, American Geophysical Union, pp.1-26.
- Smith, D.K., Cann, J.R., 1992. The role of seamount volcanism in crustal construction at the Mid-Atlantic Ridge (24°–30°N). *J. Geophys. Res.* 97, 1645–1658.
- Smith, D.K., Cann, J.R.. 1993. Building the Crust at the Mid-Atlantic Ridge. *Nature* 365, 707-715.
- Smith, W.H.F., Sandwell, D.T., 1997. Global seafloor topography from satellite altimetry and ship depth soundings. *Science* 277, 1956-1962.
- Sandwell, D.T, Smith, W.H.F., 1997. Marine gravity anomaly from geosat and ERS-1 altimetry, *J. Geophys. Res.* 102, 10039-10054.
- Tucholke, B.E., Schouten, H., 1989. Kane Fracture Zone. *Mar. Geophys. Res.* 10, 1-40.
- Wessel, P., Smith, W.H.F., 1991. Free software helps map and display data, *Eos Trans. AGU*, 72, 445-446.

## 9. Figure legends

**Fig. 1.** Colour coded seafloor image generated from the swath bathymetry data. The image is illuminated from  $45^\circ$ . Thick black line represents identified ridge axis. Blue lines across the ridge axis marked as P1 to P6 represent selected profiles shown with magnetic model, magnetization and depth in Fig. 4. TF and FZ indicate the transform fault and fracture zone respectively. Off-axis trace of the discontinuities defining the ridge segments are indicated by white lines. The dotted line on either side of the ridge axis represents line joining magnetic Anomaly 2. Square symbols denotes the location of dredge sampling, red indicates recovery of mantle rocks, and green indicates recovery of fresh basalts. a) Study area (shaded box) marked on the satellite derived gravity (Sandwell and Smith, 1997) map along with bathymetric contours (Smith et al., 1997). b) Cruise tracks over the surveyed segment of the Carlsberg Ridge.

**Fig. 2.** a) Bathymetry and magnetization profiles along the line following magnetic Anomaly 2 on the northeastern flank of the ridge axis. The red line indicates the along-axis crustal magnetization retrieved from the magnetization solution shown in Fig. 5. b) Along axis bathymetry retrieved along the line following the center of the inner valley floor joining the deeps. Anomalous along axis depth maxima are indicated by dotted circle. Redline indicates the crustal magnetization. The square symbols indicate dredge locations, symbol colour notation as in Fig.1. NTD represents non-transform discontinuity and TF denotes the transform fault. c) Same as (a) on the southwestern flank of the ridge axis. See Fig. 1 for profile locations. d) Segment wise average half spreading rate with along-axis bathymetry. Blue dashed line represents half spreading rate over the northeast flank, red dashed line represents half spreading rate over the southwest flank.

**Fig. 3.** Magnetic anomalies plotted perpendicular to the survey tracks. Thick black line represent ridge axis. Red, blue and green lines represent identified magnetic anomalies J, 2 and 2A respectively, CA represents central anomaly. Off-axis trace of the discontinuities defining the ridge segments are indicated by black dashed lines. Thick blue dashed lines represent pseudofaults indicative of ridge propagation, identified based on swath bathymetry. Other symbols are as in Fig.1.

**Fig. 4** Seafloor spreading magnetic models. Bathymetry (B), synthetic magnetic anomaly, observed magnetics reduced to pole (thick line, A), and crustal magnetization (M) along selected transects P1 to P6 (see Fig. 1 for location). Zero level is indicated by horizontal line along the profile plots of magnetic anomaly (A) and magnetization (M). Horizontal line along the bathymetry profile (B) represent 3000 m depth level. NTDs represents non-transform discontinuities, TF represents transform fault. Numbers with arrows indicate half spreading rate in mm/yr.

**Fig. 5.** Magnetization solution derived using three-dimensional inversion of the magnetic data using multibeam bathymetry grid. CA represents central anomaly and numbers represent identified magnetic anomalies. Identified axial volcanic ridges are indicated by closed contours with tick marks. Other symbols are as in Fig.1.

**Fig. 6.** Colour coded morphotectonic map along with 500 m depth contours. Red, blue and green lines represent identified magnetic anomalies J, 2 and 2A respectively.

Thin blue line and the black lines represent bathymetric highs and lows respectively. The red arrows indicate the along axis depth maxima observed over the Segment II. Other symbols are same as in Fig. 1.

Table-1. Brief description of the rocks recovered using chain-bag dredge.

Sr. No.	Latitude (N)	Longitude (E)	Depth (m)	Lithology
1.	03° 55.643'	63° 14.386'	3976	1, 2 – Fresh basalts with 2-3 mm glass.
2.	03° 06.964'	65° 44.150'	2862	
3.	03° 47.066'	63° 16.416'	2403	3, 4 - Basalts with veneer of Fe-Mn oxides.
4.	03° 52.420'	63° 31.080'	2080	
5.	03° 48.910'	63° 21.031'	4400	5, 6, 7, 8 – Fresh pillow basalts
6.	03° 47.283'	63° 28.977'	3600	9 - Serpentinites with different macroscopic characters.
7.	03° 54.704'	63° 03.375'	3012	
8.	04° 13.977'	62° 40.769'	3768	10 - Pillow Basalts, coarse grained gabbro & Serpentinites + peridotites with large (~3 mm) phenocrysts of orthopyroxenes in altered serpentine groundmass.
9.	03° 42.574'	63° 50.560'	3800	
10.	03° 48.829'	63° 06.511'	3446	

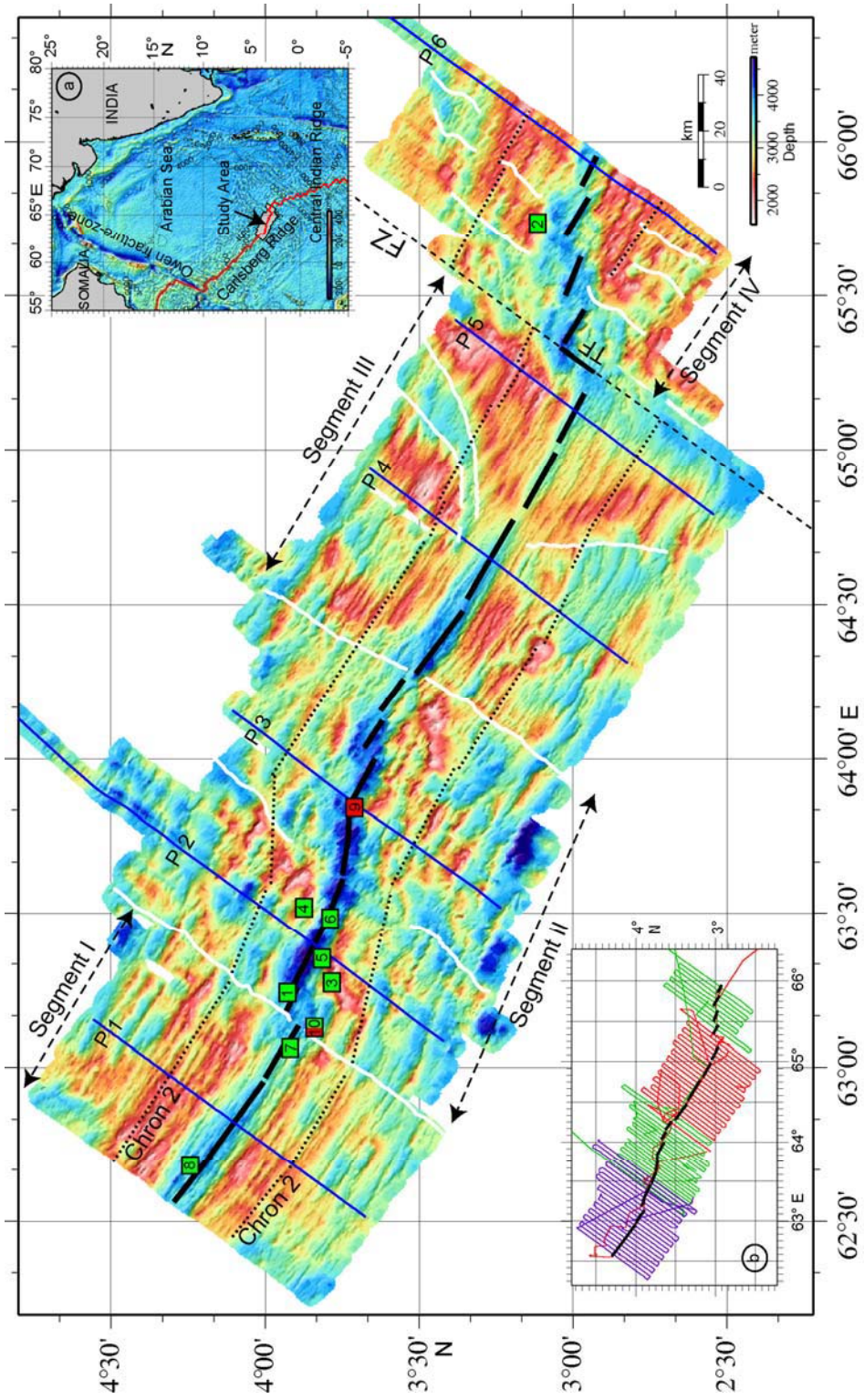


Fig. 1.  
Kamesh Raju et al., 2008



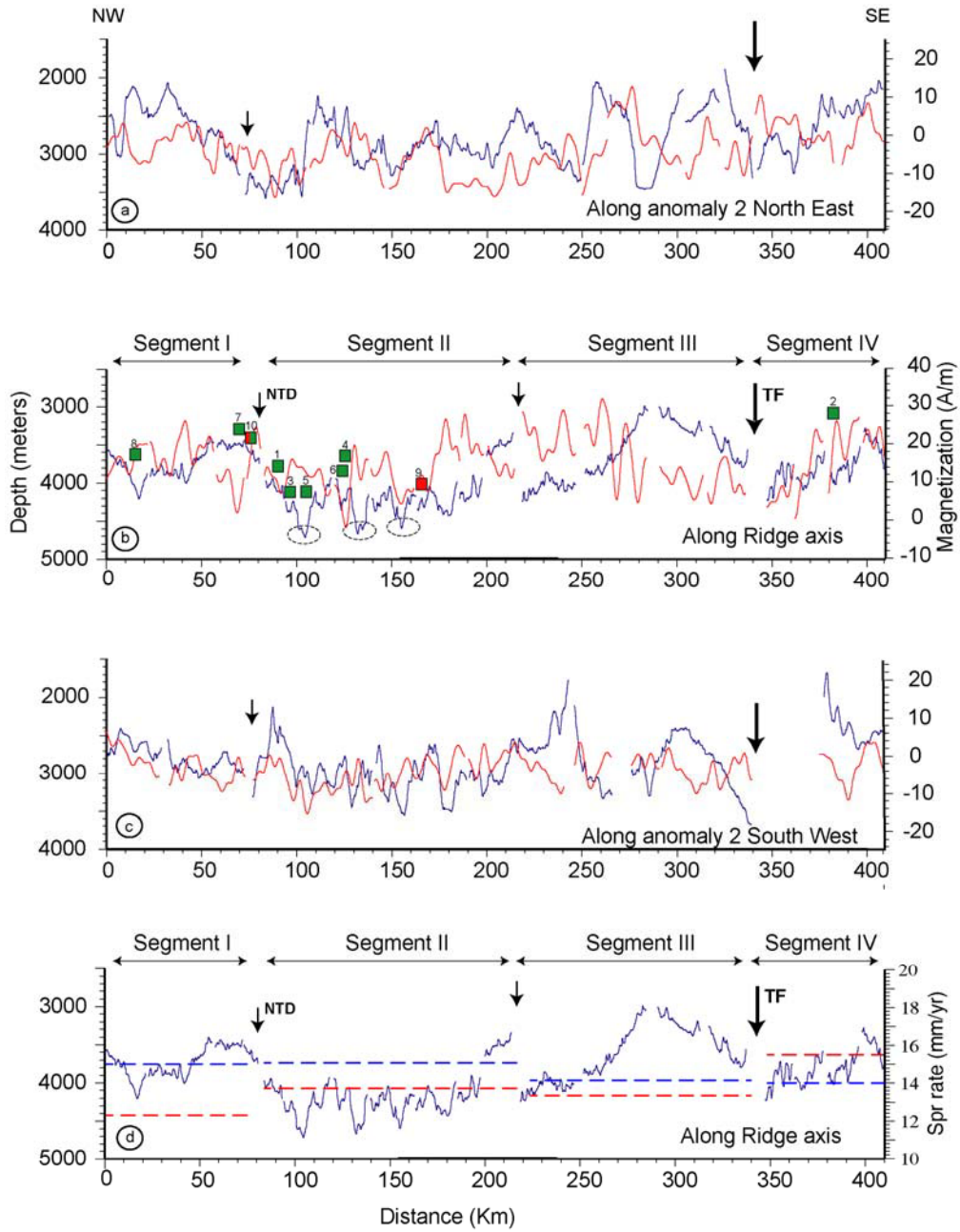


Figure- 2  
Kamesh Raju et al., 2008

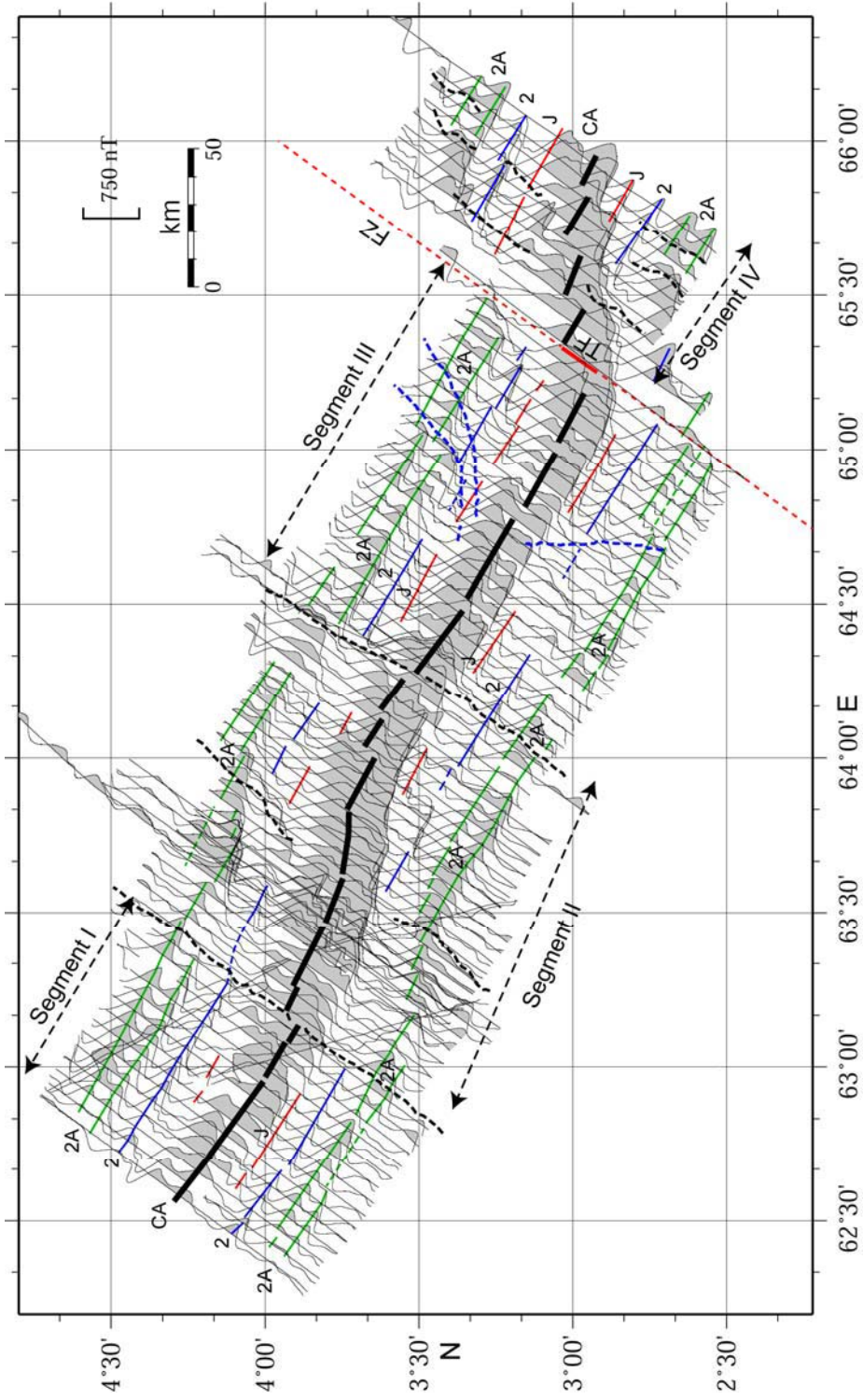


Fig. 3.  
Kamesh Raju et al., 2008

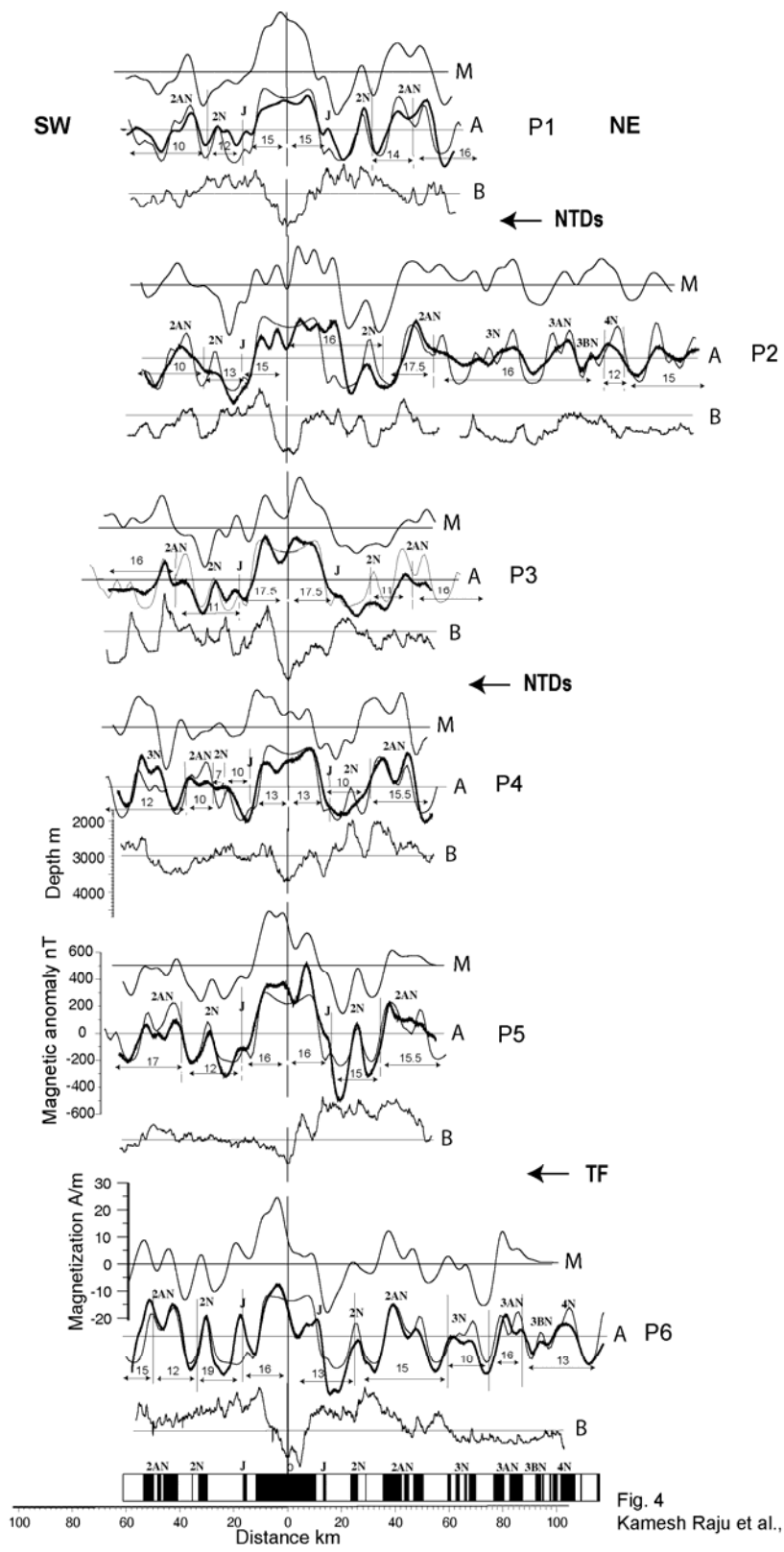


Fig. 4  
Kamesh Raju et al., 2008

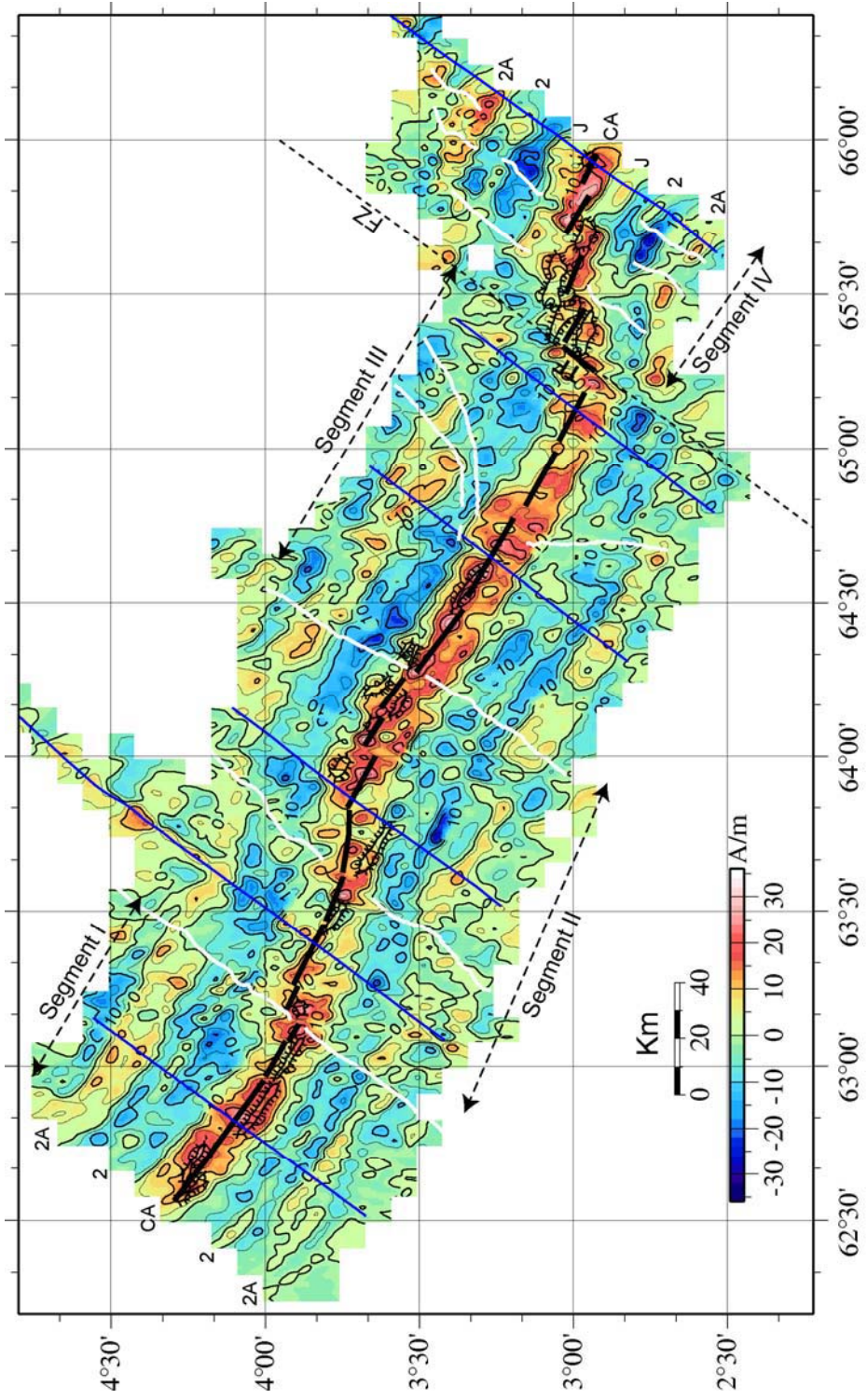


Fig. 5.  
Kamesh Raju et al., 2008



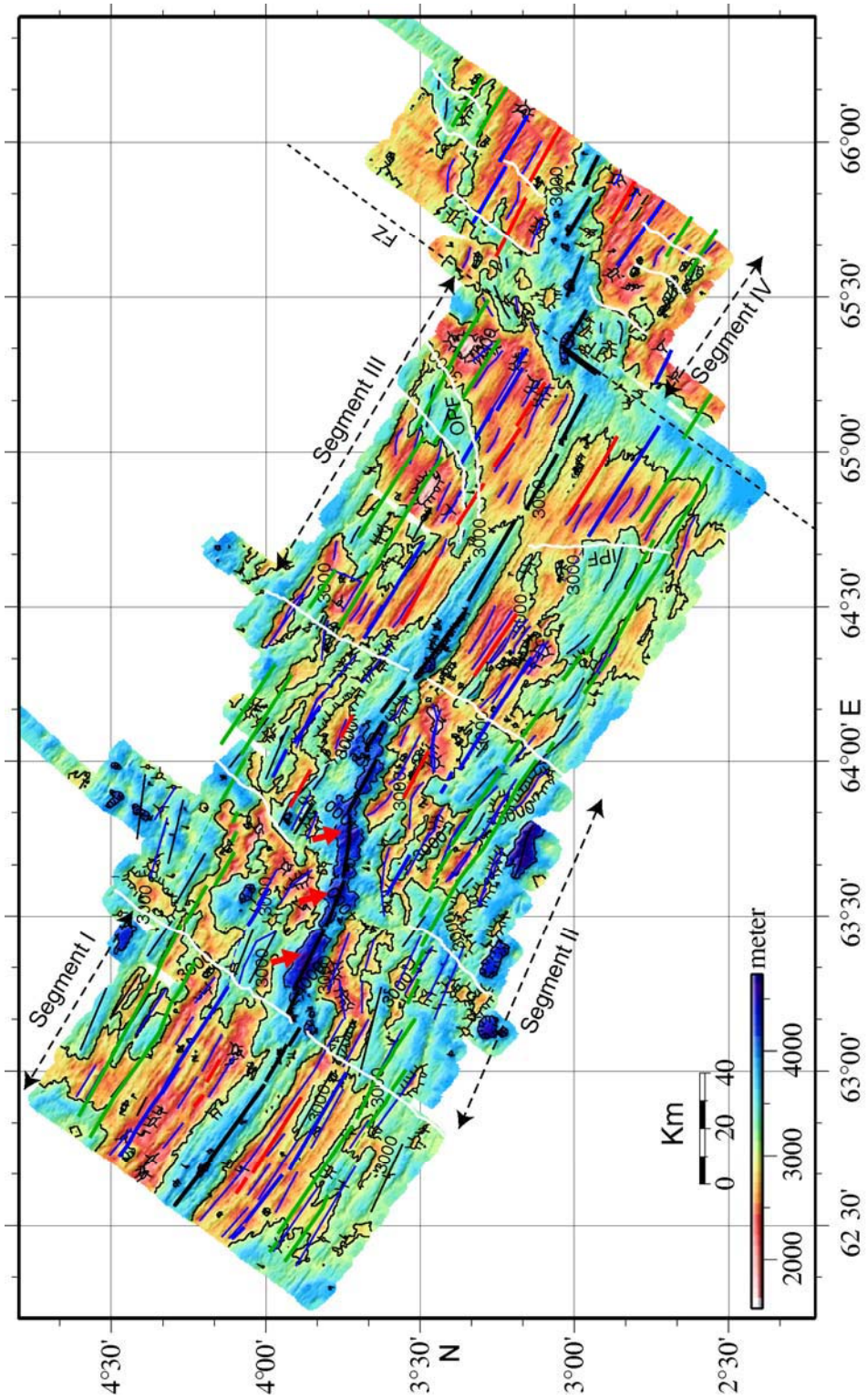


Fig. 6.  
Kamesh Raju et al., 2008